Tomographic analysis of neutron and gamma pulse shape distributions from liquid scintillation detectors at Joint European Torus

L. Giacomelli, S. Conroy, G. Gorini, L. Horton, A. Murari, S. Popovichev, D. B. Syme, and JET EFDA Contributors

AIP | Review of Scientific Instruments

Tomographic analysis of neutron and gamma pulse shape distributions from liquid scintillation detectors at Joint European Torus

L. Giacomelli, S. Conroy, G. Gorini, L. Horton, A. Murari, S. Popovichev, D. B. Syme, and JET EFDA Contributors

Citation: Review of Scientific Instruments **85**, 023505 (2014); doi: 10.1063/1.4864122
View online: http://dx.doi.org/10.1063/1.4864122
View Table of Contents: http://scitation.aip.org/content/aip/journal/rsi/85/2?ver=pdfcov
Published by the AIP Publishing

Tomographic analysis of neutron and gamma pulse shape distributions from liquid scintillation detectors at Joint European Torus

L. Giacomelli,[1,2] S. Conroy,[1,3] G. Gorini,[2] L. Horton,[1] A. Murari,[1] S. Popovichev,[1] D. B. Syme,[1] and JET EFDA Contributors[1,a)]
[1]*JET-EFDA, Culham Science Centre, Abingdon, OX14 3DB, United Kingdom*
[2]*Department of Physics, Università degli Studi di Milano-Bicocca, Milano, Italy*
[3]*Department of Physics and Astronomy, Uppsala University, Uppsala, Sweden*

(Received 4 November 2013; accepted 16 January 2014; published online 12 February 2014)

The Joint European Torus (JET, Culham, UK) is the largest tokamak in the world devoted to nuclear fusion experiments of magnetic confined Deuterium (D)/Deuterium-Tritium (DT) plasmas. Neutrons produced in these plasmas are measured using various types of neutron detectors and spectrometers. Two of these instruments on JET make use of organic liquid scintillator detectors. The neutron emission profile monitor implements 19 liquid scintillation counters to detect the 2.45 MeV neutron emission from D plasmas. A new compact neutron spectrometer is operational at JET since 2010 to measure the neutron energy spectra from both D and DT plasmas. Liquid scintillation detectors are sensitive to both neutron and gamma radiation but give light responses of different decay time such that pulse shape discrimination techniques can be applied to identify the neutron contribution of interest from the data. The most common technique consists of integrating the radiation pulse shapes within different ranges of their rising and/or trailing edges. In this article, a step forward in this type of analysis is presented. The method applies a tomographic analysis of the 3-dimensional neutron and gamma pulse shape and pulse height distribution data obtained from liquid scintillation detectors such that n/γ discrimination can be improved to lower energies and additional information can be gained on neutron contributions to the gamma events and vice versa. [http://dx.doi.org/10.1063/1.4864122]

I. INTRODUCTION

Neutron counters and spectrometers based on organic liquid scintillation materials are of common use in nuclear physics experiments.[1,2] The detector material consists of NE213 or, in most recent years, the equivalent BC501A.[3] Liquid scintillation detectors are sensitive to both neutron and gamma radiation.

At the Joint European Torus (JET, Culham, UK), the neutron emission profile monitor KN3 contains both NE213 detectors and plastic scintillation detectors.[4,5] Depending on the plasmas produced in JET, i.e., Deuterium (D) or Deuterium-Tritium (DT), the most optimal detector type can be selected. NE213 is the choice for the diagnosis of 2.45 MeV neutron emission from D plasmas while thin plastic scintillation detectors are usually used for DT 14 MeV neutrons. As KN3 is close to the vessel, the detectors are shielded to reduce the effects of the strong magnetic field on the detector photomultiplier tubes (PMT).[6]

The liquid scintillation material of the detector cell is sensitive to temperature variations as is the PMT. Also the PMT may suffer from rapid variation in gain with count rate so that incoming neutrons of the same energy give rise to pulses of different size and shape. For the purpose of counting neutrons (and the accompanying induced gamma background) above an acquisition threshold, such behavior has limited impact except for neutrons of the very lowest energies.

To monitor the long term stability of the detectors a gamma radiation source is usually implemented in the setup. If neutron energy determination is the aim of the measurements, liquid scintillation detectors need to be equipped with an extra reference source to monitor any short term count rate variations during the measurements. This source can be a light emitting diode (LED) whose stability is also monitored with the gamma radiation source. If gain variations occur, the shape of radiation and LED pulses will be modified. Their correction is then obtained by comparing the areas of the LED pulse shapes to a reference average LED area obtained in nominal operational conditions and applying this correction factor to all pulse shapes recorded during the plasma discharge.[6]

The instrument response function needs also to be measured to a high level of accuracy in order to determine the neutron energy spectrum from the analysis of the measured neutron pulse height spectrum (i.e., the distribution of the integral area of the pulses) which is extracted from the data.[7]

A new compact spectrometer (KM12) based on BC501A liquid scintillation material was installed at JET in 2010.[3,8] The detector cell is a cylinder of 2.54 cm diameter and 2.54 cm thickness equipped with a LED control and monitoring system. With suitable high voltage settings of the PMT, KM12 allows for measurement of neutron energy in the range 1–20 MeV such that it can be used as a compact broadband neutron spectrometer to measure simultaneously the 2.45 MeV and 14 MeV neutrons from D and DT plasmas. KM12 has already demonstrated such capability by measuring 14 MeV neutrons due to triton burn-up fusion reactions

[a)] See the Appendix of Romanelli *et al.*, Proceedings of the 24th IAEA Fusion Energy Conference, San Diego, USA, 2012.

in D plasmas during high power shots of JET experimental campaign C27.[8–10] Measurements of instrument response function, detector setup, and calibration were performed at the Physikalisch-Technische Bundesanstalt (PTB, Braunschweig, Germany).[11]

Both KN3 and KM12 instruments implement the same type of digital data acquisition system based on 200 MSample/s 14-bit digitizers capable of count rate up to 5×10^5 Cps designed by ENEA Frascati (Italy).[8,12]

II. TOMOGRAPHIC ANALYSIS TECHNIQUE FOR n/γ PULSE SHAPE DISCRIMINATION

Organic liquid scintillation material is sensitive to both neutron and gamma radiation. Neutrons and gammas induce different excited states of the organic molecules which decay with mechanisms which give rise to pulses of different shape.[13] Specifically, gamma radiation generates sharp pulses whereas neutron pulse shapes feature wider trailing edges due to the longer decay time constant of the molecular excited states. Various techniques have been developed to discriminate neutron (n) and gamma (γ) radiation for this type of detectors with similar success.[14–16]

The easiest and most common n/γ discrimination method is the gate method which consists of integrating the radiation pulse shape within ranges (i.e., gates) of different duration along the pulse, i.e., on the rising and/or trailing edges.[14,17,18]

In the past, this method was implemented directly in analogue acquisition systems with the use of pulse shape discrimination units as the earlier KN3.[4,5] The analogue units feature various controls to set the optimal n/γ pulse shape discrimination using either an AmBe source installed in KN3 or the direct radiation emitted from JET plasma discharges. The units give separate output pulse streams for neutrons and gammas. In contrast, the availability of digital acquisition systems has allowed recording the pulse shapes of the incoming radiation as a sequence of digital pulse amplitude values (in mV) which can then be software analyzed off-line when the measurement is complete.

Since the installation of the new digitizers,[8,12] algorithms were developed to process KN3 and KM12 digital data either to remove offsets induced by the noisy measurement environment or to identify pile-ups in the recorded pulse shapes. In case of KM12, data are also corrected for PMT gain variations using LED pulse shapes as a reference.

The gate method is adopted for n/γ pulse shape discrimination of KN3 and KM12 digital data. It allows for the comparison of the integrals (i.e., areas) calculated within ranges of different width along the pulse shapes. The comparison is typically represented in terms of the whole pulse area (i.e., the Total gate proportional to the radiation deposited energy inside the detector) with respect to the ratio of the areas obtained integrating each pulse within two optimal gates (i.e., Short and Long gates). A study for assessing the optimal gate width and combinations was pursued for the analysis of both KN3 and KM12 data according to Ref. 18. In this case, the optimal gates of 15 ns (Short) and 70 ns (Long) are measured along the pulse trailing edge from the peak of radiation pulse shape such that the Short/Long ratio <1.[18] Since neutron pulse shapes feature wider trailing edges than gammas, neutrons give rise to lower Short/Long ratios. As an example, all the shots from KM12 neutron spectrometer measured during JET experimental campaigns C28-C30 with ITER-like wall[19,20] were processed in order to extract the neutron and gamma radiation emitted from D plasmas during the auxiliary heating phase only. The gamma radiation is generated from neutron interactions in the tokamak structure, from plasma impurities and from the KM12 ^{207}Bi reference source. The result of the gate method analysis can be represented as a 3-dimensional pulse shape distribution of Short/Long ratio vs. radiation deposited energy referred to as PSD throughout the article as is displayed in Figure 1. The figure also displays the LED pulse shape distribution arising from the KM12 control and monitoring system. In the data processing to account for PTM gain variations, the pulse shapes are LED corrected. The correction proves to be satisfactory to the level of the LED resolution of about 2.5% (full width at half maximum) as for individual shots.[6,8] Due to triton burn-up fusion reactions in D plasmas 14 MeV neutrons are visible in the PSD as well.[8–10]

The discrimination of neutrons and gammas in the PSD can be achieved by setting up a separation line (magenta line in Figure 1). The quality of the separation depends on the liquid scintillation material, on its age and on the radiation deposited energy. As can be seen from Figure 1, if the triggering threshold of the data acquisition is high (i.e., deposited energy >1000 keVee), neutrons and gammas are well separated. The impact of the analysis method and the optimization of its parameters are then very limited. The n/γ discrimination is easily achieved, the corresponding neutron and gamma pulse height spectra can then be determined and further analyzed to obtain, specifically, the profile of the plasma neutron emission for KN3 and the neutron energy spectrum for KM12.

The n/γ discrimination becomes more difficult for radiation of low energy (i.e., the pulse height). For example, the first Compton edge usually falls within a few hundreds of

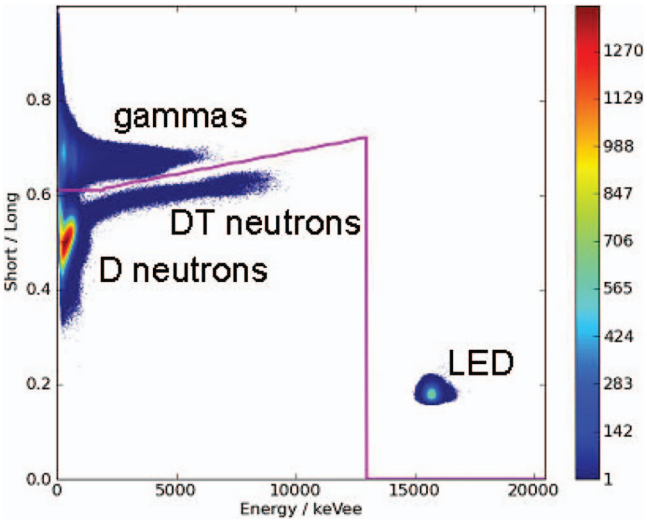

FIG. 1. KM12 PSD distribution of Short/Long gates vs. radiation deposited energy (proportional to the Total gate) obtained for just the heating phase of all shots of JET experimental campaign C28-C30 (5.7×10^7 events). The magenta n/γ separation line is defined visually.[8]

keVee and its measurement is important to monitor the detector stability, to define the energy scale and the detector efficiency. Moreover, depending on the PMT gain setting, a good compromise has to be achieved between measuring low energy neutrons and gammas and, at the same time, minimizing the contribution of spurious noise of energy-downgraded radiation in this region.

Low energy neutrons and gammas induce similar pulse shapes in liquid scintillation detectors. These end up in the region of deposited energy below 1000 keVee of Figure 1. Here, neutron and gamma events overlap and a separation line, usually set visually, would just rigidly discriminate the two types of events.

To improve the n/γ discrimination in this low energy region, a further step in the PSD analysis obtained with the gate method has be taken using a tomographic technique to find the locus of the minimum in the pulse shape separation between accumulated neutrons and gamma events at each total energy.[21] The tomographic analysis consists of slicing the PSD distribution into arbitrary energy ranges, in which the corresponding Short/Long distribution can be determined and studied individually. For this, specific algorithms were designed in Fortran and Python.[22,23] For each slice relative to a radiation energy range, the minimum point between the two lobes of the Short/Long distribution is determined (see magenta vertical line in Figure 2). The minimum defines the coordinates of the separation line in that specific PSD slice.

The model was first developed for the gamma radiation obtained from the reference ^{207}Bi source of KM12.[8] Various distribution functions were used for comparison with the data using a Python script to implement the minimization of normalized Cash statistics (C),[24] which theoretically should result in $C = 1$ if the model perfectly matches the data. In this study, the various models were compared in terms of mean value and width of the distribution of the C values from the model comparison to the data of each PSD slice. The best results were obtained using the sum of a Rayleigh function and a constant representing the background level (b): $f(A, \mu, \sigma, b) = A\frac{x}{\sigma^2}e^{\frac{-(x-\mu)^2}{2\sigma^2}} + b$ where A is the amplitude, μ the mean value and σ the standard deviation of the Rayleigh function, and x the bin number of the Short/Long distribution within [0, 1] of the PSD slice. With the gamma model in place, the analysis focused on the Short/Long distributions of the PSD obtained for neutron and gamma measurements as displayed in Figure 1. Here, instead of using for the neutron lobe the same model developed for gamma radiation independently, the combination of two Rayleigh functions and a constant background (Double Rayleigh model) proved to give a good representation of the data compared to other distribution functions such as Gaussian and Log-normal functions (see yellow line for the Double Rayleigh model in Figure 2). In case of convergence of the model to large values of C (i.e., $C > 10$), which might happen for Short/Long distributions of PSD slices where the event density is low (i.e., $\ll 1$ event per bin), the number of free parameters is reduced to only amplitudes and/or standard deviations. The initial conditions of the parameters for the model comparison are set using the maximum amplitudes and positions of the neutron and gamma lobes of the Short/Long distribution. Once the Double Rayleigh model converges to a reasonable C value, the individual Rayleigh functions can be extracted and used to represent the neutron and gamma lobes of the Short/Long distributions. To fit the LED component in the PSD which is already well separated from neutrons and gammas, the linear combination of two Gaussian functions and a constant background (Double Gaussian model) is used.

The tomographic analysis of the whole PSD distribution allows for an accurate definition of the n/γ separation locus and for the identification of low energy neutron and gamma contributions in the overlapping region such that the individual neutron and gamma distributions can be reconstructed and used to determine the specific pulse height spectra.

This type of analysis can be pursued for PSD slices of radiation deposited energy of different width which would then affect both the statistics of the Short/Long distribution

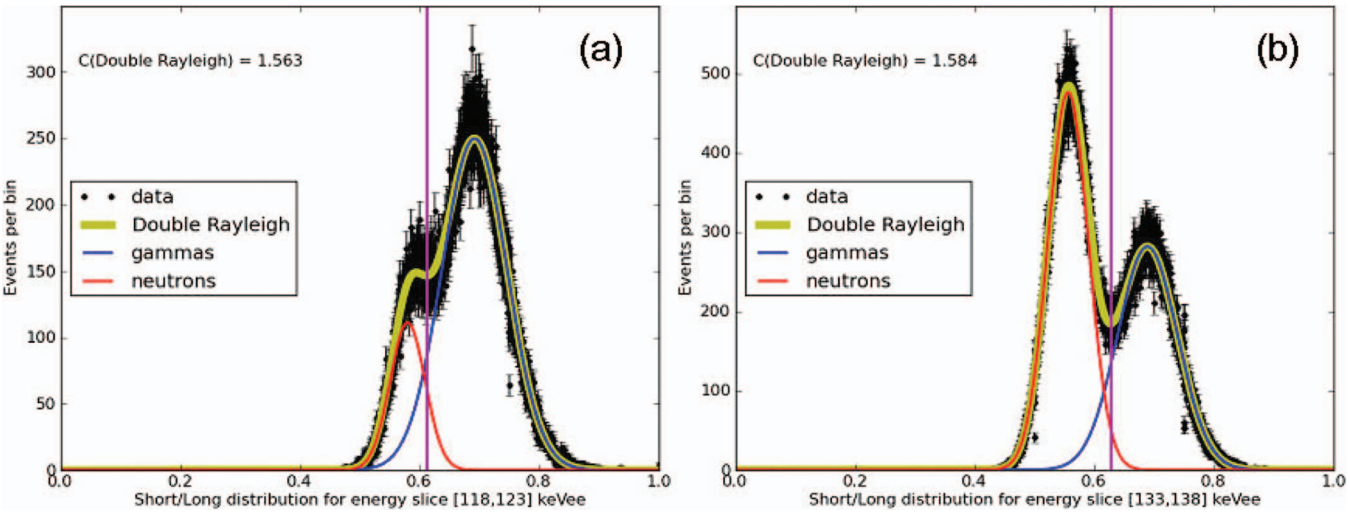

FIG. 2. Short/Long distributions obtained from the PSD shown in Figure 1 for radiation energy deposited about 120 keVee and 135 keVee. They are compared to the Double Rayleigh model (yellow line) in terms of Cash statistics C. The magenta vertical line corresponds to the local minimum of model and it is used as n/γ separation point in that specific PSD slice. The red and blue lines represent the individual Rayleigh distribution of the neutron and gamma lobes.

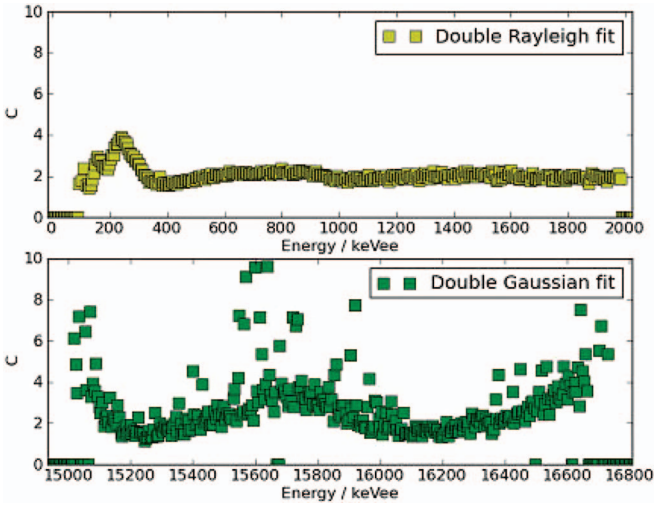

FIG. 3. Results of radiation and LED models comparisons in terms of Cash statistics *C*.

for the model comparison to the data and the accuracy (energy step) of the separation line between neutrons and gammas. The tomographic analysis presented here is run for PSD energy slices of 5 keVee which is the width of the energy bin of the KM12 response function.[11]

Figure 2 shows examples of the Double Rayleigh model comparison obtained for PSD slices of radiation deposited energy about 120 keVee and 135 keVee and of the definition of the minimum point of the Short/Long distribution. The local minimum of the model defines the coordinates of the accurate n/γ separation line for that specific PSD energy range. The neutron and gamma lobes are then obtained from the model as individual Rayleigh distributions. If the comparison converges, the model is normalized to the data to preserve the total number of PSD events.

The quality of the tomographic analysis relies upon a good selection of the model functions adopted for the data comparison and it is assessed in terms of Cash statistics which should converge to $C = 1$ in case of perfect representation of the data (Figure 3).

The trend for the Double Rayleigh model is quite flat about $C = 2$ which is the best values obtained compared to the other models. About 250 keVee, C values give rise to a peak which rapidly decays. This region corresponds to radiation events of low energy, above the data acquisition threshold but lower than the first ^{207}Bi Compton edge.[25] Concerning the LED model comparison shown in the bottom panel of Figure 3, the trend features larger C values at the extremes corresponding to the wings of the LED energy distribution with <70 events per bin in the PSD slices. At about 15 650 keVee, C is about 10 with some scattering due to the event density of the specific LED distributions. These results achieved with the Double Gaussian model are much better than those obtained using only one Gaussian function (plus background) which C is a factor of 10 larger at 15 650 keVee.

III. RESULTS ON THE TOMOGRAPHIC ANALYSIS OF KM12 PULSE SHAPE DISTRIBUTION

The tomographic analysis was developed using PSD's with good statistics. First, the distribution model was determined considering the gamma PSD from the KM12 ^{207}Bi reference source. Then, two PSD's were produced considering KM12 digital data recorded during heating and ohmic phases of all the D plasma shots performed in JET experimental campaigns C28-C30. The heating phase PSD corresponds to 5.7 $\times$ 10^7 events while the ohmic phase PSD to 1.7 $\times$ 10^7 events. Figures 4 and 5 display the n/γ separation line defined using the PSD tomographic analysis for the heating and ohmic phase PSD's, respectively.

The separation line is determined from the local minimum of the Double Rayleigh model in each specific energy range the PSD is divided while the neutron and gamma

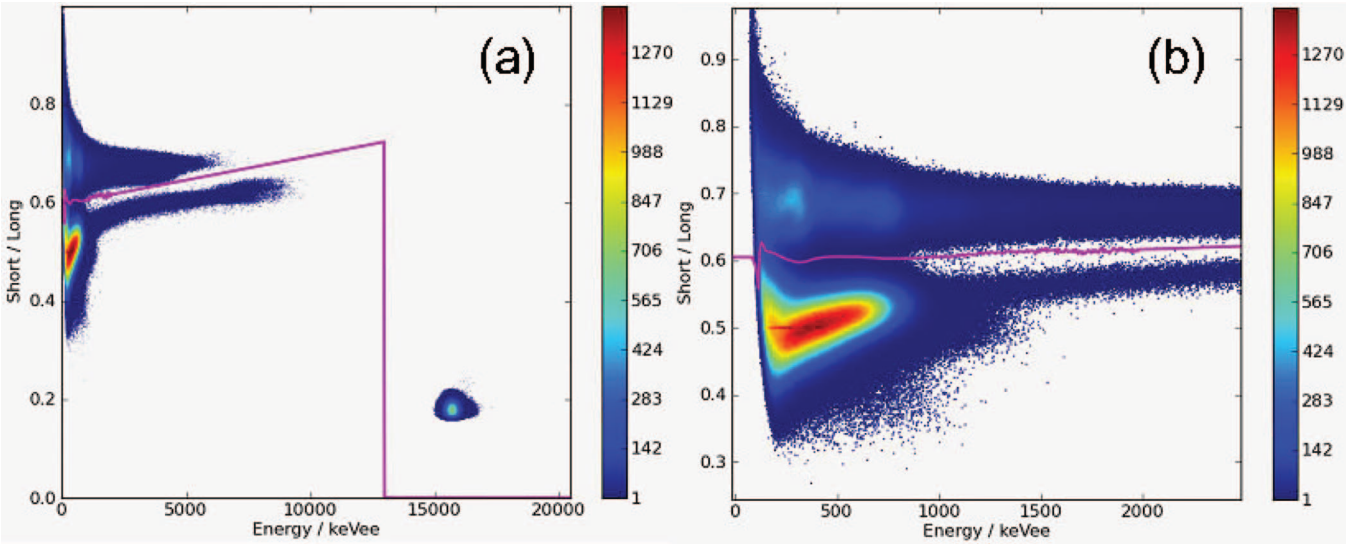

FIG. 4. KM12 heating phase PSD of 5.7 $\times$ 10^7 events (a) and a detail (b) showing the separation line (magenta) for n/γ discrimination using tomographic analysis.

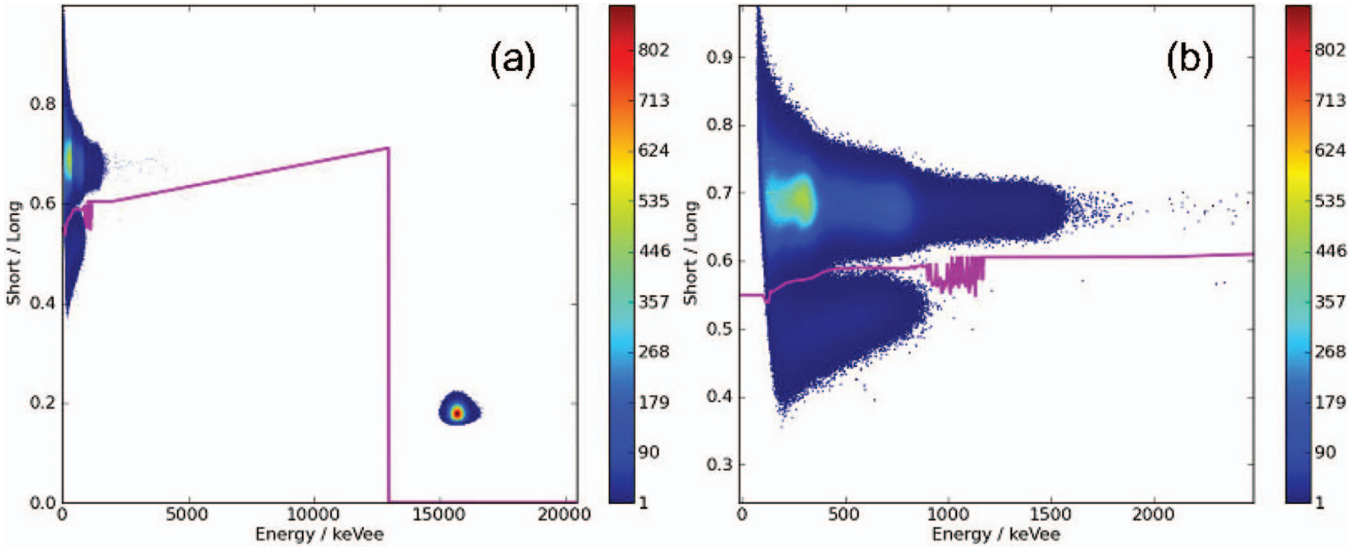

FIG. 5. As Figure 4 but for the ohmic phase PSD of 1.7×10^7 events.

lobes of the Short/Long distribution are obtained from the individual Rayleigh functions of the model and allow for the assessment of the neutron and gamma contributions in the overlapping region about the minimum.

The tomographic analysis results in the determination of the individual neutron and gamma PSD's from the Double Rayleigh model. For instance, the PSD for the heating phase is composed of 4.1×10^7 neutrons, 1.1×10^7 gammas, and 4.8×10^6 LED events as displayed in Figures 6 and 7. The

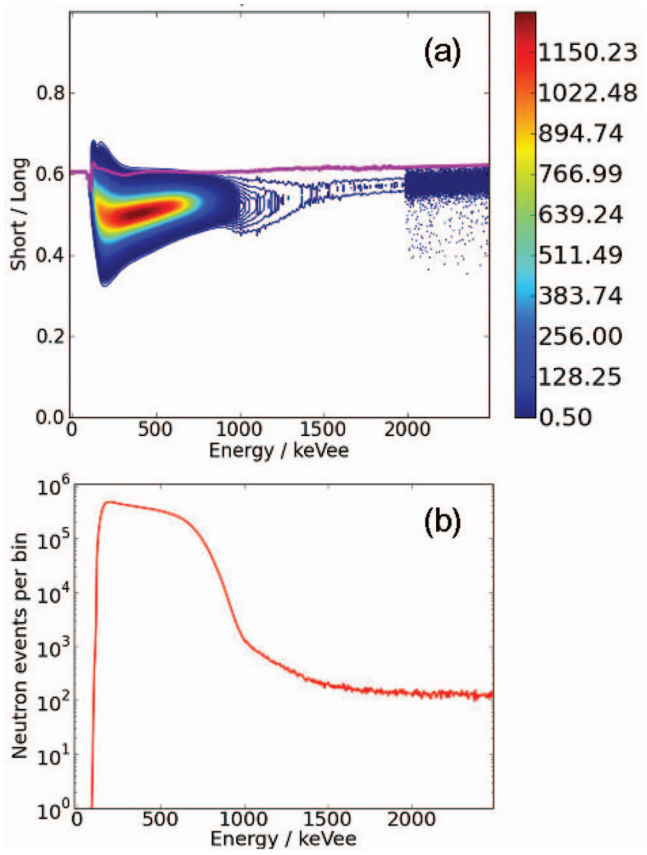

FIG. 6. Tomographic reconstructed KM12 neutron PSD for the heating phase of JET experimental campaigns C28-C30 (4.1×10^7 events). In (a), the neutron contribution into the gamma region is visible above the n/γ separation line (magenta) with $R = 0.2\%$. The color scale is relative to model amplitudes. In (b), the corresponding neutron pulse height spectrum as a projection of the neutron PSD onto the energy axis in log scale.

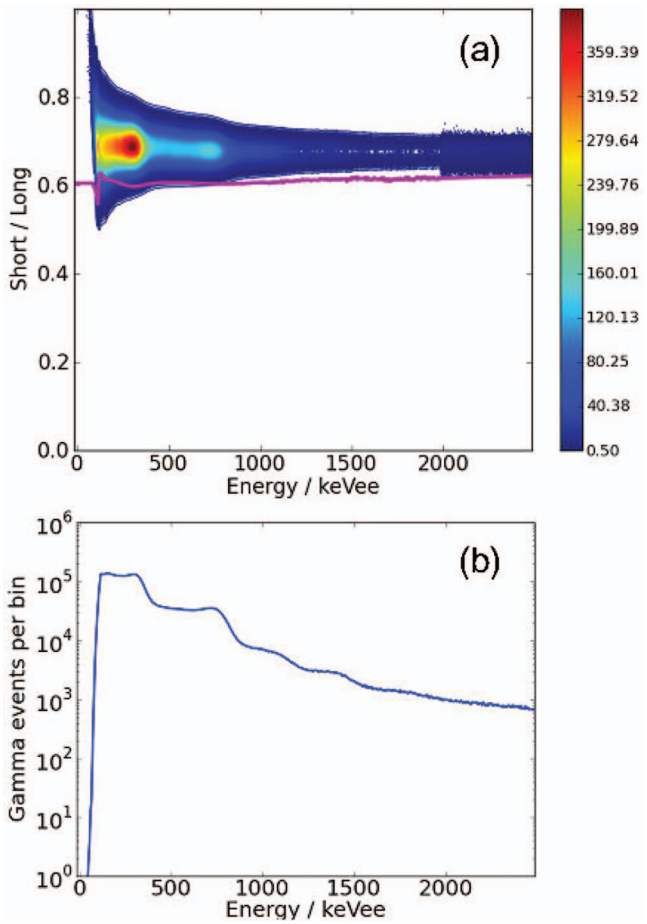

FIG. 7. As Figure 6 but for gammas (1.1×10^7 events) where $R = 1.9\%$ are identified as being in the neutron region.

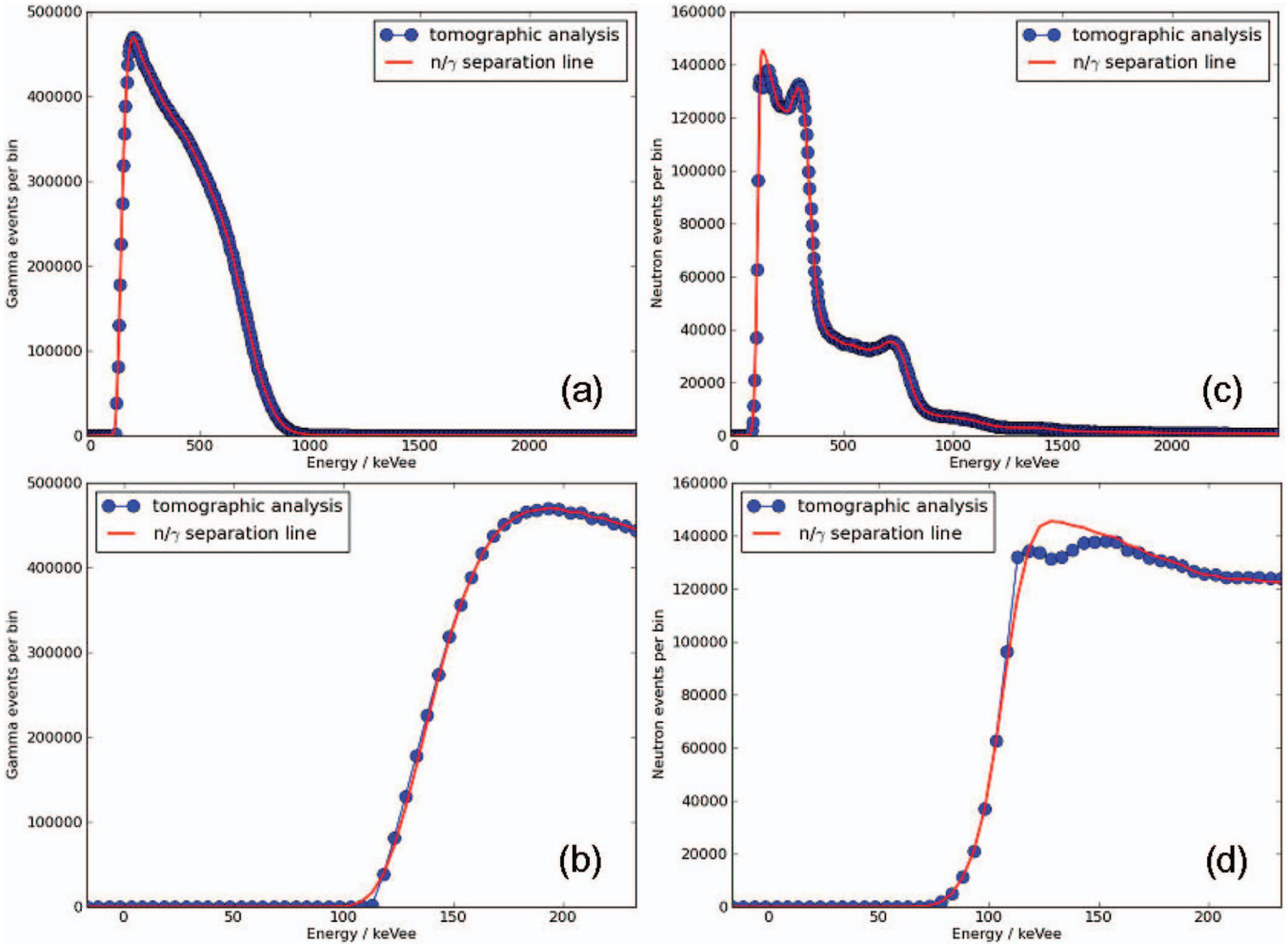

FIG. 8. Comparison of the neutron (a) and gamma (c) pulse height spectra of the heating phase PSD (Figure 4(a)) obtained using the tomographic analysis and the n/γ separation line of Figure 1. A magnification of the spectra low energy region is shown in panels (b) and (d), respectively.

amount of identified events in the overlapping region of the PSD on one side of the n/γ separation line can be compared to the total number of certain events on the other side of the n/γ separation line through their ratio R. This highlights the identified event fraction with respect to a rigid n/γ separation as shown in Figure 1. In this case, $R = 0.2\%$ for neutrons and $R = 1.9\%$ for gammas.

Figure 6(a) shows a discontinuity at about 1000 keVee energy which corresponds to the maximum deposited energy of energetic neutrons above 2.45 MeV generated by accelerated D ions fusion reactions during the heating phase. The tomographic reconstruction reproduces the step in this energy region of the neutron event distribution of the heating phase PSD visible in Figure 4(b) where the number of neutron events drops by one order of magnitude. Another discontinuity is recognizable at 2000 keVee of the reconstructed neutron and gamma PSD's of Figures 6 and 7. Although the Double Rayleigh model comparison could be pursued up to 6000 keVee (see Figure 4(a)), neutrons and gammas are already well separated above 2000 keVee (see Figure 4(b)) and there is no need of a model comparison. Real neutron and gamma data are used for the tomographic reconstruction above 2000 keVee. A similar analysis was carried out for the ohmic PSD whose neutron pulse height spectrum will be used to verify the energy resolution of the KM12 spectrometer at JET.[26] This spectrum contains 4.8×10^5 neutrons ($R = 1.6\%$), 9.8×10^6 gammas ($R = 0.04\%$), and 6.5×10^6 LED events.

Figure 8 displays the comparison between the tomographic reconstructed neutron and gamma pulse height spectra from the heating phase PSD with respect to the ones obtained using the n/γ separation line defined visually in Figure 1. The difference relates to the low energy events below 150 keVee. The tomographic analysis identifies the neutron contribution into the low energy gamma region (Figure 8(c)) and vice versa with an impact on the slope of the pulse height spectra in the region of the data acquisition threshold. In this case, the difference is limited to 3467 events and affects the region about 110 keVee as visible in Figures 8(b) and 8(d).

The tomographic analysis was then carried out also for individual JET shots. Specifically, shots 83 550 and 83 551 are the ones featuring the highest neutral beam injected (NBI) power of JET experimental campaign C30 with 25.65 MW

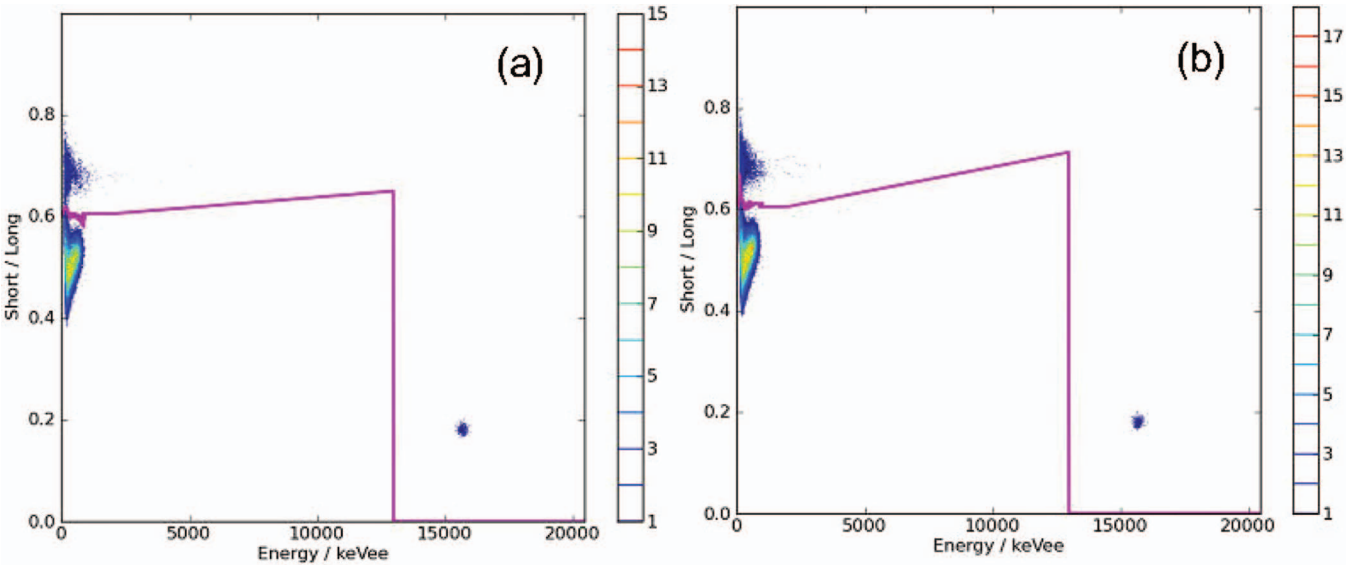

FIG. 9. PSD of shots 83 550 (a) and 83 551 (b) during 49.5–52.3 s of NBI steady phase. The total number of events is 2.0×10^5 and 2.7×10^5, respectively, of which 3.0×10^3 are due to the LED control and monitoring system.

and 25.5 MW, respectively. The analysis was pursued during a specific time interval of these shots (49.5–52.3 s) where the NBI heating was stable and KM12 reached a maximum neutron count rate of 7.5×10^4 Cps with averages of 6.2×10^4 Cps for neutrons and 8.9×10^3 Cps for gammas. For the definition of the n/γ separation line, the same initial Short/Long value of 0.6 as for the KM12 heating phase PSD was used. Figure 9 shows the PSD distributions of shots 83 550 and 83 551.

The minimization of Cash statistics for the radiation and LED models proved to be a very robust method when the tomographic analysis was pursued for the time sliced data of shots 83 550 and 83 551. Here, although the statistics of the Short/Long distributions is low, the models comparison converges and allow for similar analysis as for the heating and ohmic cases. Figures 10(a) and 10(c) show a flat trend of C for both shots 83 550 and 83 551 which is about 2 for the most of the PSD energy slices. The high statistics-low energy and low statistics-high energy regions features an increase of C up to 3 and 6 for shot 83 550 (Figure 10(a)) while it is steeper up to 10 for shot 83 551 (Figure 10(c)). The C values for the Double Gaussian model analysis of the LED of the PSD distributions are displayed in Figure 10(b) and 10(d) and are similar for the two shots. The reconstructed neutron PSD with the identification of the neutron events falling into the gamma region is displayed in Figure 11.

The total number of events KM12 measured within the NBI power steady state of shot 83 550 corresponds to 2.0×10^5 whose 1.7×10^5 are neutron events ($R = 0.2\%$) and 3.0×10^3 are LED events. The gamma events are

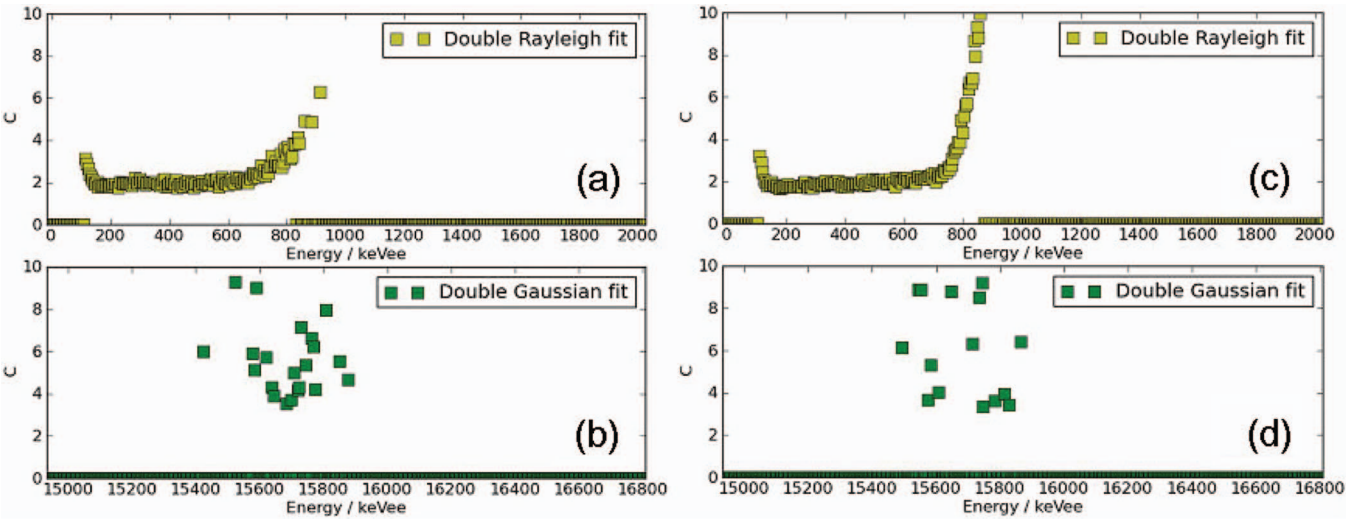

FIG. 10. Results of radiation and LED models comparison in terms of Cash statistics C for shots 83 550 ((a) and (b)) and 83 551 ((c) and (d)) during the NBI steady phase (49.5–52.3 s).

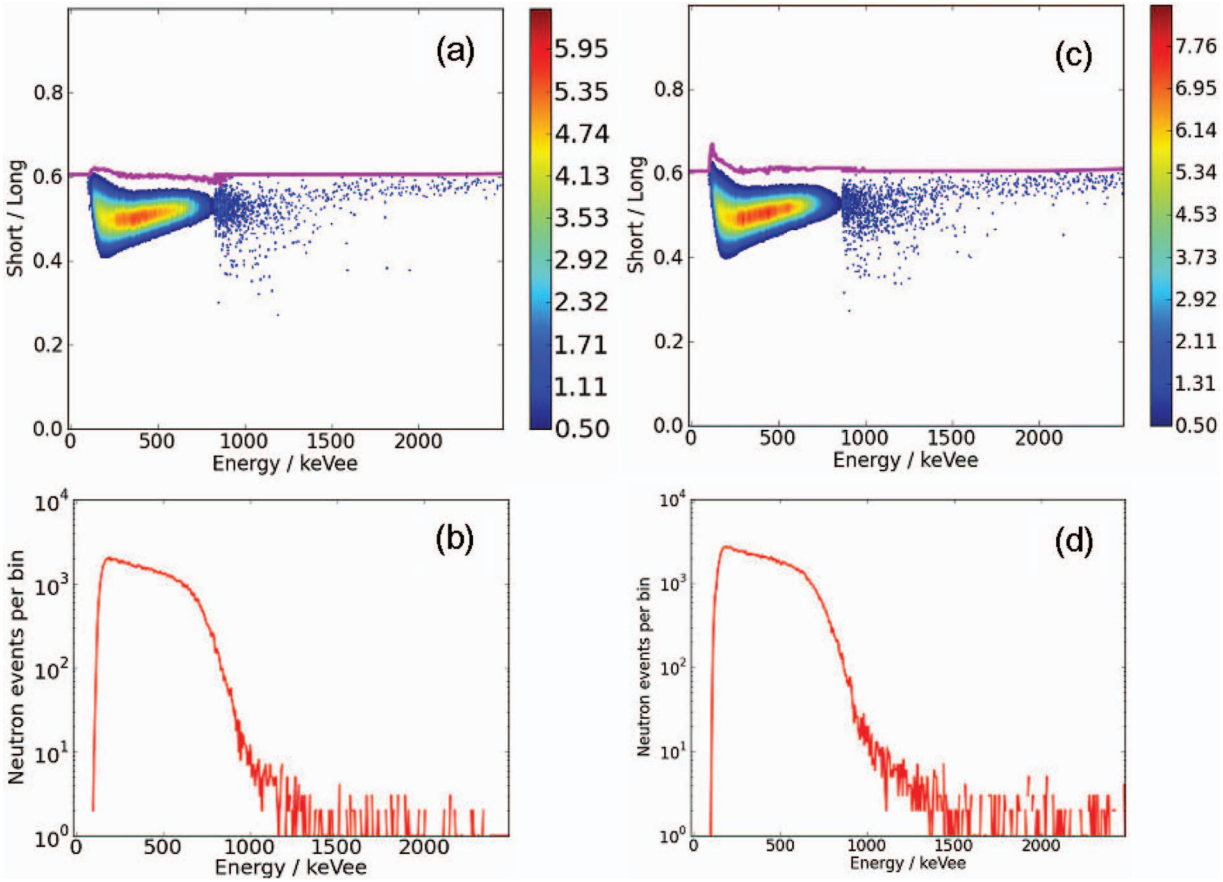

FIG. 11. Tomographic reconstructed KM12 neutron PSD for shot 83 550 (a) extracted from the PSD displayed in Figure 9(a). The color scale is relative to model amplitudes. In (b), the corresponding neutron pulse height spectrum in log scale. Panels (c) and (d) display similar results for shot 83 551 (Figure 9(b)).

2.2×10^4 and R results 2.3%. For shot 83 551 instead, 2.4×10^5 are neutron events ($R = 0.1\%$) and 2.5×10^4 are gamma events ($R = 5.4\%$).

To attain the neutron energy spectrum relative to these specific plasma conditions, the neutron pulse height spectrum will be further analyzed making use of the measured KM12 response function.[11,27]

The tomographic analysis presented here is carried out for ranges of radiation deposited energy of 5 keVee. In principle also the opposite could be pursued, i.e., slicing the PSD in terms of Short/Long ratios. This choice, however, is much more complex in view of the shape of the neutron lobe of the PSD distribution (see Figures 4, 5 and 9). The distribution of neutron deposited energies <1000 keVee in KM12 spectrometer (typical of 2.45 MeV neutron emission from D plasmas) is slanting and it grows towards the gamma lobe for higher neutron energies. This means that, differently from gamma interactions, the response of organic liquid scintillation materials depends on the energy of the incoming neutrons. Neutrons emitted in D plasmas can make single or multiple scattering on Hydrogen and Carbon nuclei or induced p(n,γ)D reactions with the production of 2.2 MeV gammas. The scattered protons or Carbon nuclei are responsible for the transitions of the organic molecules of the scintillation material to different excited states from which they decay through the specific scintillation light emission.[13] For neutron energies larger than 5 MeV, inelastic scattering on Carbon and the products of ^{12}C(n,n′)3α and ^{12}C(n,α)^{9}Be reactions can also contribute to the scintillation process.[28] This type of tomographic analysis would require a much more complex modeling especially for the identification of the events in the PSD overlapping region for specific Short/Long slices.

IV. RESULTS ON THE TOMOGRAPHIC ANALYSIS OF KN3 PULSE SHAPE DISTRIBUTION

The tomographic analysis was then carried out for KN3 data. The KN3 NE213 detectors were installed in early 1990s and they do not implement a LED monitoring system.[4,5] The gamma reference source is ^{22}Na (about 10^2 Cps). Figure 12 shows the PSD KN3 channel 15 measured during the shot 83 550 steady NBI phase. The detector measured a maximum neutron count rate of 1.3×10^5 Cps, 77% higher with respect to KM12, with averages of 1.1×10^5 Cps for neutrons and 1.3×10^4 Cps for gammas.

The Double Rayleigh model set up for KM12 was then tested on KN3 data. Here, in view of the specific response of the scintillator detectors, which is different from each other and from KM12 one, particular efforts have been devoted to adjust the number of free parameters of the model and the initial conditions for the comparison. Figures 13 and 14 show

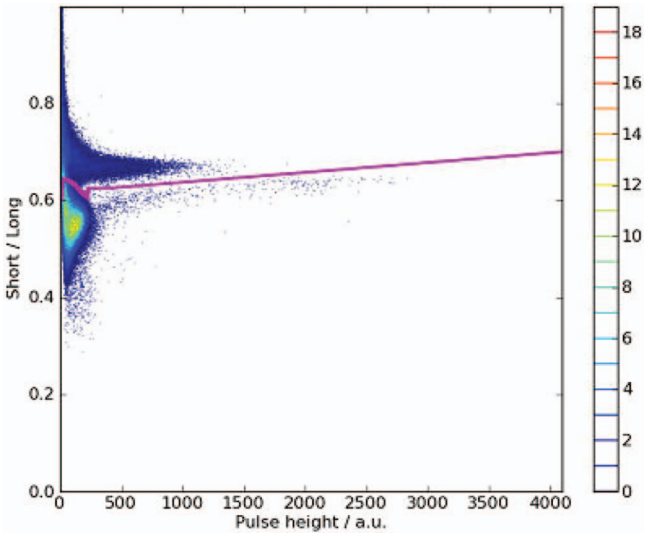

FIG. 12. KN3 channel 15 PSD of shot 83 550 during 49.5–52.3 s of NBI steady phase. The total number of events is 3.4×10^5.

the results in terms of Cash statistics and tomographic reconstructed neutron PSD and pulse height spectrum of 2.8×10^5 events with $R = 1.2\%$ neutrons identified in the gamma region (see Figure 15).

The amount of identified neutrons and gammas in the overlapping PSD region of each KN3 channel is presented in Figure 15 in terms of ratio R. Depending on the line of sight, efficiency, age, and performance of each KN3 counter, the PSD's feature different shapes resulting in different degree of separation of neutrons and gammas. The KN3 detectors at the edge are exposed to higher gamma background with respect to the central channels. The trend of gamma R depends on the shape of the converging Double Rayleigh model whose gamma component is smaller than the neutron one but wider into the neutron region such that a relative higher number of gamma events are identified in the overlapping region of the PSD.

The profile of the counts measured in each KN3 channels induced by neutron and gamma radiation emitted from NBI steady phase of shot 83 550 is shown in Figure 16. The neutron and gamma emission profiles will then be obtained considering the efficiency and attenuation of the KN3 detectors along each individual line of sight: This work requires modeling and calculations which are in progress.

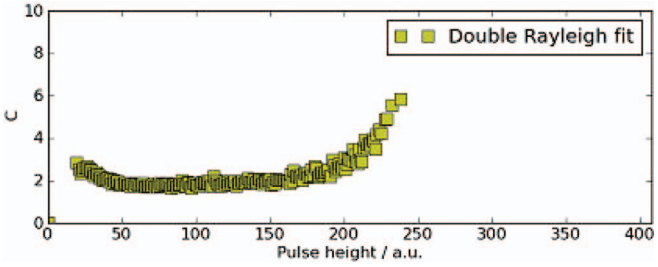

FIG. 13. KN3 channel 15 results of Double Rayleigh model comparison in terms of Cash statistics C for shot 83 550 during the NBI steady phase (49.5–52.3 s).

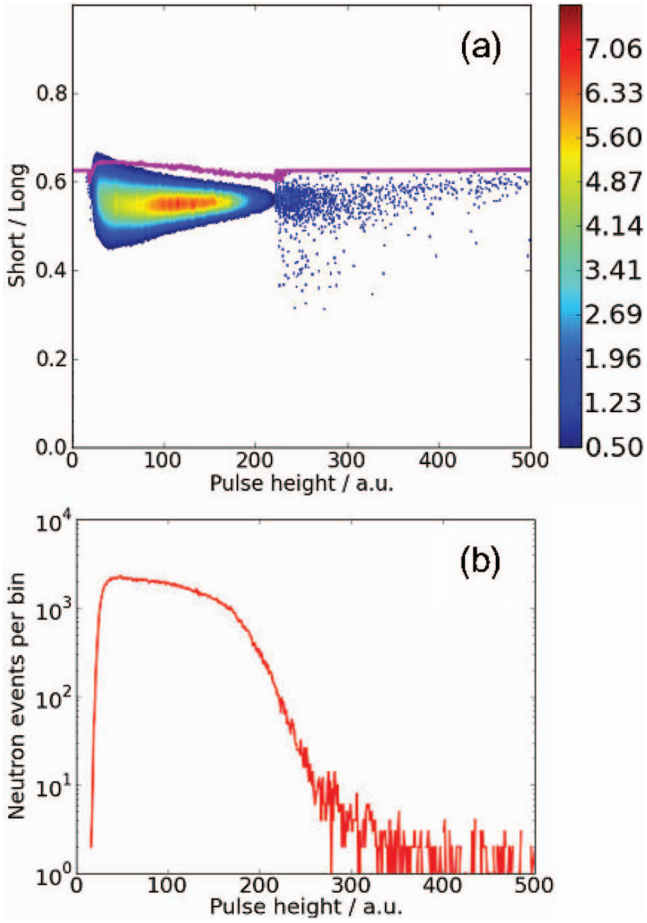

FIG. 14. As Figure 11 but for KN3 channel 15 with 2.8×10^5 neutron events ($R = 1.2\%$).

V. OBSERVATIONS UPON KN3 PERFORMANCE

The installation of the new fast digital data acquisition system[12] has improved the KN3 count rate capability up to $<5 \times 10^5$ Cps compared to about 3×10^4 Cps of the old analogue acquisition system demonstrated already in shot 83 550. To

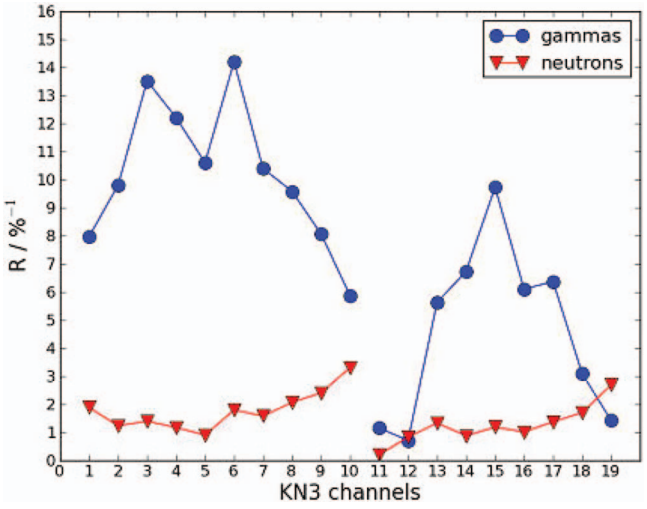

FIG. 15. Event ratio R for each KN3 channel relative to the NBI steady phase of shot 83 550.

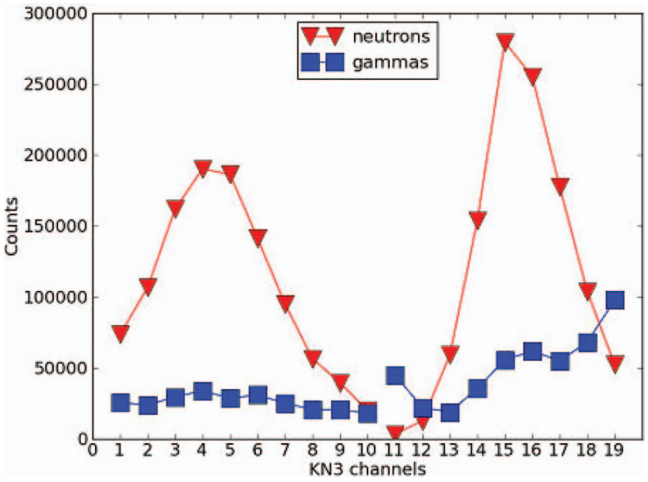

FIG. 16. Profile of neutron and gamma counts KN3 measured during the NBI steady phase of shot 83 550.

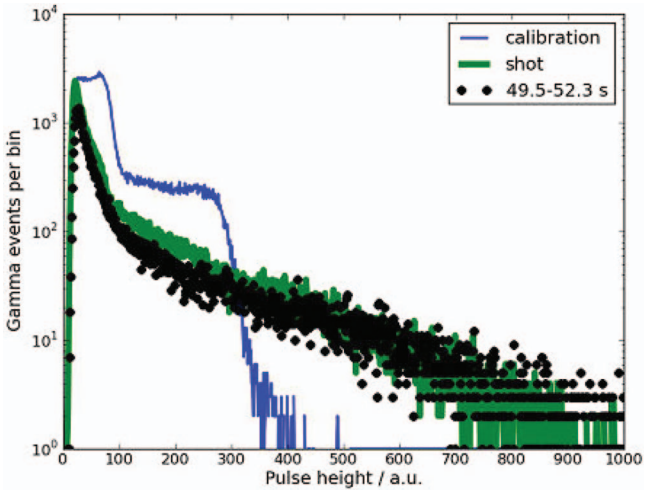

FIG. 17. KN3 channel 15 gamma pulse height spectra measured during the calibration, the shot and for 2.8 s of the NBI steady phase of shot 83 550.

prove the count rate limit higher auxiliary heated D plasmas need to be produced as planned for the coming experimental campaigns at JET.

As mentioned before, the KN3 NE213 detectors PMTs can be sensitive to count rate variations and there is no information upon their behavior in such conditions. Count rate variations would modify the pulse shapes induced by radiation events of the same characteristics. For instance, neutrons of the same energy but emitted with different intensity during the plasma discharge result in measured pulse height spectra of different shape. This would hamper the interpretation of the neutron and gamma emission profile for specific plasma conditions. An experiment upon the dependence of the pulse height spectrum on the count rate was carried out under controlled conditions at the PTB accelerator for the BC501A cell and PMT of the KM12 neutron spectrometer.[29] Accelerated deuterons were beamed on a tritiated target to produce 14 MeV neutrons. The KM12 spectrometer was placed at different distances from the target to vary its count rate and prove the capability of its digital acquisition system and the reliability of the data correction of its LED control and monitoring system. The neutron pulse height spectra corresponding to count rate measurements of 1.2×10^4 Cps, 1.5×10^5 Cps, and 4.2×10^5 Cps were compared. The LED corrected neutron spectra are similar for the first two measurements within 0.1%. The 4.2×10^5 Cps measurement induced a PMT gain drift of 23% but the corresponding neutron pulse height spectrum obtained after LED correction was similar to the one of 1.2×10^4 Cps to within 1.1%.[29]

The KN3 detectors do not implement a LED control monitoring system. In principle, a first order correction could be applied using the ^{22}Na reference source. If the Compton edges of the ^{22}Na gamma spectra measured in each KN3 detector during the calibration routinely performed in between shots (nominal conditions) and during the specific plasma time interval could be compared, the measured neutron pulse height spectrum could be corrected for the PMT gain drift. Figure 17 displays a comparison of the ^{22}Na gamma pulse height spectrum in KN3 channel 15 measured during the calibration for 2389.0 s before shot 83 550, during the whole shot 83 550 (120.5 s) and for the specific time interval of its NBI steady phase (49.5–52.3 s).

The ^{22}Na Compton edges of the calibration pulse height spectrum are well defined before the shot while during the shot most of the gammas measured are induced by neutron interaction in the tokamak structure or from D plasma impurities. A hint of the first ^{22}Na Compton edge is visible for the pulse height spectrum for the whole shot at about 100 a.u. In these conditions the comparison and correction mentioned before cannot be carried out.

For these reasons, the installation of new gamma reference sources of higher activity together with a LED control and monitoring system to the 19 counters of KN3 would be beneficial to achieve reliable diagnosis of the plasma neutron profile emission and fully exploit the capability of the new digital data acquisition system. However, this task is not easy due to design constraints of the KN3 detectors whose cells lack the opening for the required optical fibers. Furthermore, in view of the age of the NE213 scintillation cells installed in the early 1990s, it would be easier to replace all KN3 counters with detectors of performance similar to the KM12 neutron spectrometer. In this case, for the KN3 horizontal and vertical central channels (i.e., 4–6 and 14–16, respectively) it is recommended to couple new BC501A cells with PMTs which are insensitive to gain drifts up to 10^6 Cps to maintain the LED correction efficient for high count rate measurements.[30] These KN3 channels could be then energy calibrated as for KM12. A similar upgrade of KN3 would allow for spectroscopic information along the individual view lines such that the neutron emission of plasma ion populations of different temperature can be also identified.

Concerning DT experiments, calculations to assess neutron rates for various D:T density ratios plus direct, scattered, and background radiation levels are necessary to verify the possible performance of the upgraded KN3 instrument.

If achievable, a spectroscopic neutron camera operational at JET would be an important test in view of the design and operation of the ITER neutron camera and of the capability of a similar instrument for DEMO.[31,32]

VI. CONCLUSIONS

A further step in the use of the gate method of n/γ pulse shape discrimination for liquid scintillation detectors has been presented. This consists of the tomographic analysis of the PSD through the comparison of model functions to the Short/Long distribution obtained considering ranges of radiation deposited energies through the minimization of Cash statistics. The method was developed first for the KM12 neutron spectrometer and then adapted to the 19 counting detectors of the neutron emission profile monitor KN3. The tomographic analysis allows the identification of the contribution of neutrons in the gamma region of the PSD and achieves a better accuracy in the definition of the pulse height spectra which is useful to set the data acquisition thresholds and to define the detector efficiency.

From the analysis of these spectra the energy (for KM12) and the profile (for KN3) of the plasma neutron emission can be obtained. The tomographic method is general and robust and can be applied to the analysis of other types of data in the form of PSD distributions.

For KN3, the overlapping region of neutrons and gammas in the PSD is wider. This follows from the age of the detectors (more than 20 years old), the lines of sight, and the effects of PMT gain variations which cannot be LED corrected. A proposal to upgrade KN3 to spectroscopic capability is also mentioned in the article to exploit the performance of its new digital data acquisition system and of the tomographic analysis hereby presented.

ACKNOWLEDGMENTS

The authors are grateful to colleagues of ENEA Frascati (Italy) and PTB Braunschweig (Germany) laboratories for the precious work and fruitful collaboration and to D. Simpson, M. Beldishevski, P. Heesterman, and P. Blanchard for their support at JET. This work was supported by EURATOM and carried out within the framework of the European Fusion Development Agreement. The views and opinions expressed herein do not necessarily reflect those of the European Commission.

[1]H. Klein and S. Neumann, Nucl. Instrum. Methods Phys. Res. A **476**, 132 (2002).
[2]R. Nolte, M. S. Allie, P. J. Binns, F. Brooks, A. Buffler, V. Dangendorf, J. P. Meulders, F. Roos, H. Schuhmacher, and B. Wiegel, Nucl. Instrum. Methods Phys. Res. A **476**, 369 (2002).
[3]See http://www.detectors.saint-gobain.com/uploadedFiles/SGdetectors/Documents/Product_Data_Sheets/BC501-501A-519-Data-Sheet.pdf for BC501A properties.
[4]J. M. Adams, O. N. Jarvis, G. J. Sadler, D. B. Syme, and N. Watkins, Nucl. Instrum. Methods Phys. Res. A **329**, 277 (1993).
[5]M. J. Loughlin, N. Watkins, J. M. Adams, N. Basse, N. P. Hawkes, O. N. Jarvis, G. Matthews, F. B. Marcus, M. O'Mullane, G. Sadler, J. D. Strachan, P. van Belle, and K.-D. Zastrow, Rev. Sci. Instrum. **70**(1), 1123 (1999).
[6]L. Giacomelli, A. Zimbal, K. Tittelmeier, H. Schuhmacher, G. Tardini, and R. Neu, Rev. Sci. Instrum. **82**, 123504 (2011).
[7]L. Bertalot, S. Conroy, A. Murari, M. Reginatto, H. Schuhmacher, and A. Zimbal, in *32nd EPS Conference on Plasma Phys., Tarragona, 27 June–1 July 2005* (ECA, 2005), Vol. 29C, P-1.078, see http://epsppd.epfl.ch/Tarragona/pdf/P1_078.pdf.
[8]F. Belli, S. Conroy, B. Esposito, L. Giacomelli, V. Kiptily, A. Lücke, D. Marocco, M. Riva, H. Schuhmacher, B. Syme, K. Tittelmeier, and A. Zimbal, IEEE Trans. Nucl. Sci. **59**(5), 2512 (2012).
[9]G. Gorini, L. Ballabio, and J. Källne, Plasma Phys. Controlled Fusion **39**, 61 (1997).
[10]L. Ballabio, J. Frenje, J. Källne, S. W. Conroy, G. Ericsson, M. Tardocchi, E. Traneus, and G. Gorini, Nucl. Fusion **40**, 21 (2000).
[11]F. Gagnon-Moisan, M. Reginatto, and A. Zimbal, in *2nd International Workshop on Fast Neutron Detectors and Applications, Ein Gedi, Israel, 6–11 November 2011*, see http://iopscience.iop.org/1748-0221/7/03/C03023/pdf/1748-0221_7_03_C03023.pdf.
[12]M. Riva, B. Esposito, D. Marocco, F. Belli, and B. Syme, Fusion Eng. Des. **86**, 1191 (2011).
[13]G. F. Knoll, *Radiation Detection and Measurement*, 3rd ed. (Wiley, New York, 1999), p. 220.
[14]S. Marrone, D. Cano-Ott, N. Colonna, C. Domingo, F. Gramegna, E. M. Gonzalez, F. Gunsing, M. Heil, F. K. Appeler, P. F. Mastinu, P. M. Milazzo, T. Papaevangelou, P. Pavlopoulos, R. Plag, R. Reifarth, G. Tagliente, J. L. Tain, and K. Wisshak, Nucl. Instrum. Methods Phys. Res. A **490**, 299 (2002).
[15]S. Yousefi, L. Lucchese, and M. D. Aspinall, in *IEEE Nuclear Science Symposium Conference Record,* NSS '08*, 19–25 October 2008* (IEEE, 2008), p. 2387, see http://ieeexplore.ieee.org/xpl/articleDetails.jsp?arnumber=4774836.
[16]E. Ronchi, P.-A. Söderström, J. Nyberg, E. Andersson Sundén, S. Conroy, G. Ericsson, C. Hellesen, M. Gatu Johnson, and M. Weiszflog, Nucl. Instrum. Methods Phys. Res. A **610**(2), 534 (2009).
[17]M. Mardiyanto, Atom Indonesia **34**(2) (2008), see http://aij.batan.go.id/index.php/aij/article/view/101/73 for an n/γ discrimination method.
[18]L. Giacomelli, A. Zimbal, M. Reginatto, and K. Tittelmeier, Rev. Sci. Instrum. **82**, 013505 (2011).
[19]See https://www.efda.org/jet/jet-iter/iter-like-wall-project/ for the JET ITER-Like Wall project.
[20]G. F. Matthews, M. Beurskens, S. Brezinsek, M. Groth, E. Joffrin, A. Loving, M. Kear, M.-L. Mayoral, R. Neu, P. Prior, V. Riccardo, F. Rimini, M. Rubel, G. Sips, E. Villedieu, P. de Vries, and M. L. Watkins, Phys. Scr. **T145**, 014001 (2011).
[21]P. J. Ell, J. M. Deacon, D. Ducassou, and A. Brendel, Br. Med. J. **280**(6212), 438 (1980).
[22]See http://www.g95.org/ for Fortran 95 compiler.
[23]See http://www.python.org/ for Python programming language.
[24]W. Cash, Astrophys. J. **228**, 939 (1979).
[25]See http://hesperia.gsfc.nasa.gov/~schmahl/cash/cash_oddities.html for Cash statistic.
[26]A. Zimbal, M. Reginatto, H. Schuhmacher, L. Bertalot, B. Esposito, F. Poli, J. M. Adams, S. Popovichev, V. Kiptily, and A. Murari, Rev. Sci. Instrum. **75**(10), 3553 (2004).
[27]L. Giacomelli, S. Conroy, F. Belli, G. Gorini, L. Horton, E. Joffrin, E. Lerche, A. Murari, S. Popovichev, M. Riva, and B. Syme, in *International Conference on Fusion Reactor Diagnostics, Villa Monastero, Varenna, Italy*, 9–13 September 2013, see http://www.iop.org/Jet/fulltext/EFDC130402.pdf.
[28]See http://www-nds.iaea.org/exfor/endf.htm for the evaluated nuclear cross sections database.
[29]D. Marocco, F. Belli, B. Esposito, M. Riva, L. Giacomelli, M. Reginatto, K. Tittelmeier, and A. Zimbal, IEEE Trans. Nucl. Sci. **56**(3), 1168 (2009).
[30]M. Nocente, M. Tardocchi, A. Olariu, S. Olariu, R. C. Pereira, I. N. Chugunov, A. Fernandes, D. B. Gin, G. Grosso, V. G. Kiptily, A. Neto, A. E. Shevelev, M. Silva, J. Sousa, and G. Gorini, IEEE Trans. Nucl. Sci. **60**(2), 1408 (2013).
[31]See http://www.iter.org/ for the ITER project.
[32]See http://ec.europa.eu/research/energy/euratom/index_en.cfm?pg=fusion&section=tech-prep-demo for the DEMO project.